Journal of Solid State Chemistry **147,** 410–420 (1999)
Article ID jssc.1999.8465, available online at http://www.idealibrary.com on IDEAL®

In Situ Structural and Electrochemical Study of $Ni_{1-x}Co_xO_2$ Metastable Oxides Prepared by Soft Chemistry

J. M. Tarascon,* G. Vaughan,† Y. Chabre,‡ L. Seguin,* M. Anne,§ P. Strobel,§ and G. Amatucci¶

*Université de Picardie Jules Verne, Laboratoire de Réactivité et Chimie des Solides and CNRS UPRES-A 6007, 33, rue Saint-Leu, 80039 Amiens cedex, France; †ESRF, BP 200, 38043 Grenoble, France; ‡Lab. Spectrométrie Physique, UJF and CNRS, BP 87, 38402 Saint Martin d'Hères, France; §Laboratoire de Cristallographie-CNRS-BP 166, 38042 Grenoble cedex, France; and ¶Telcordia (formerly Bellcore), Red Bank, New Jersey

Received January 12, 1999; in revised form May 21, 1999; accepted July 22, 1999

Metastable $Ni_{1-x}Co_xO_2$ phases were obtained from the electrochemical deintercalation of lithium from the precursor phases, $LiNi_{1-x}Co_xO_2$ ($x = 0$, 0.3, and 1), using plastic electrochemical cells. The structural changes induced during Li removal, together with the thermal stability of the end members $Ni_{1-x}Co_xO_2$, were determined by *in situ* X-ray measurements using a high-resolution synchrotron beam line. The advantages of using a plastic battery configuration to perform such a study is emphasized. The structural/thermal stability results are discussed in relation to the electrochemical performance of these materials. Numerous changes in the unit cell symmetry were observed during deintercalation. The NiO_2 end member is described with a single distorted CdI_2-type structure, while two CdI_2-type structures, both with reduced O–O interlayer distances, but differing by the presence of oxygen vacancies, are needed to describe the CoO_2 end member. The reduction in O–O spacing is explained by partial polymerization within oxide frameworks. Such a behavior, already observed with layered chalcogenides, can be explained on the basis of the elegant electron-hole chemistry pioneered by J. Rouxel who directly evidenced the role of the anion during an intercalation process.

INTRODUCTION

Soft chemistry is mainly used to prepare metastable phases, involving numerous types of low-temperature synthesis reactions, such as ion exchange, acid–base reactions, or electrochemical reactions. Herein we will mainly focus on materials synthesized via electrochemical deinsertion of Li. Such reactions are mainly pseudomorphous (e.g., the particle shape is maintained during the reaction) and topotactic (e.g., there is a structural filiation between the precursor phase and the obtained metastable phase, (1, 2).

The layered $LiMO_2$ (M = Co, Ni) oxides are among the most studied intercalation compounds because of their great interest with respect to the field of energy storage. Today's commercial Li-ion cells have $LiCoO_2$ as the positive electrode (3); however, for safety and performance reasons such a material is only used up to 50% of its theoretical capacity. Until recently, attempts to trap more capacity from this electrode by chemical or electrochemical means have failed due to the lack of chemical oxydants and highly resistant electrolytes against oxidation, respectively. The exceedingly strong repulsive forces between the negatively charged $(Co/Ni)O_2$ layers, which develop once the Li ions acting as screening ions are removed, were claimed to be at the origin of the inability to prepare the Li_0NiO_2 and Li_0CoO_2 phases (4, 5). While this fact was becoming well accepted, Amatucci *et al.* (6) reported the electrochemical preparation of the CoO_2 and NiO_2 members from $LiCoO_2$ and $LiNiO_2$, respectively. They showed that upon Li removal, the basic structural framework was preserved with the ability for these Co/NiO_2 phases to convert back to $LiNiO_2$ and $LiCoO_2$ phases by reintercalating one lithium ion. CoO_2 was found to be layered with a CdI_2 structure, whereas NiO_2 retains the $CdCl_2$ structure of $LiNiO_2$.

Although Amatucci *et al.* (6) succeeded in indexing the end-members series with an hexagonal unit cell, the limited intensity and resolution of conventional X-ray sources used prevented them from unraveling the structural details that could account for the stability of the NiO_2 and CoO_2 end members. Several mechanisms, such as the existence of Co vacancies resulting from Co dissolution, the migration of Co ions within the Li sites, the corrugation of the CoO_2 layers, and finally the appearance of a ferroelectric distortion, were proposed to account for the NiO_2 and CoO_2 phase stabilization upon Li removal, hence, the need to further study the fundamental aspects of these materials to determine which of the proposed mechanisms governed the phase stabilization, and to propose solutions for a better use of their theoretical capacity in practical cells. To alleviate the X-ray resolution issue faced by the previous authors (6), synchrotron radiation sources that provide good statistics and high resolution to enable the detection of small variations between diffraction patterns were used. The instrumental high resolution of the powder diffractometer installed on the

0022-4596/99 $30.00

BM16 synchrotron beam line at ESRF, Grenoble, leads to a 2θ peak broadening at half maximum of 0.006° (0.06° for laboratory sources), which is negligible compared to the broadening from size and strain sample effects. In this case, the widths of the peaks due to sample broadening only ($\Gamma = X \tan\theta + Y/\cos\theta$) decrease with the wavelength, always ensuring good separation between peaks at any wavelength: the closer the lines, the narrower their widths. Thus, high resolution allows the revelation of small details of the diffraction pattern and also enables the calculation of very precise cell parameters.

It has long been recognized (7, 8), that *in situ* techniques should allow one to pin down the material chemical reactivity/structural stability limitations without the drawbacks of the *ex situ* method, namely, the risk of atmospheric contamination and the adverse effect of self-discharge. However, their use has been limited. The reason is that designing sample holders compatible with a specific experiment while maintaining hermetic seals and a properly functioning cell, is not trivial. With the introduction of the plastic Li-ion technology (9, 10), most of the *in situ* characterization techniques have been simplified. Indeed, a unique feature of this plastic battery is its construction by a hot-laminating process that allows for a high design flexibility. Electrochemical cells of any size and any shape can be assembled. Reference electrodes or heating elements can be added to this configuration, without penalty, to accurately follow the deintercalation process as a function of cycling conditions and temperatures as reported herein.

EXPERIMENTAL

In situ X-ray diffraction has been carried out on plastic $LiNi_{1-x}Co_xO_2$/C Li-ion batteries (Bellcore technology). The electrochemically active components ($x = 0$, 0.3, and 1) used in this study were synthesized in-house. $LiNiO_2$ was obtained from subsequent heatings of stoichiometric mixtures of LiOH and NiO under an oxygen flow at 700°C, while $LiCoO_2$ was prepared from LiOH and Co_3O_4 as previously reported. $Li_{1-x}Ni_{1+x}O_2$ was made as $LiNiO_2$, but the heating process was conducted under air rather than oxygen. The degree of cationic mixing in the Li layers (11, 12) (e.g., values of x) can easily be determined from XRD. Several authors have shown the intensity ratios $I(003)/I(104)$, $I(102, 006)/I(101)$ as reliable criteria for the estimation of x in $Li_{1-x}Ni_{1+x}O_2$ (e.g., Ni^{+2} within the Van der Waals gap). Using the formula proposed by Reimers *et al.* (12) involving the ratio between the integrated peak areas, we calculated the x value in our sample (Fig. 1) to be 0.058. This value implies the presence of about 6% of nickel ions between the NiO_2 layers.

Finally, appropriated amounts of LiOH, NiO, and Co_3O_4 were fired at 750°C under oxygen to prepare the mixed $Li_yNi_{1-x}Co_xO_2$ phase. The hexagonal lattice parameters for all the phases studied here are given in Table 1.

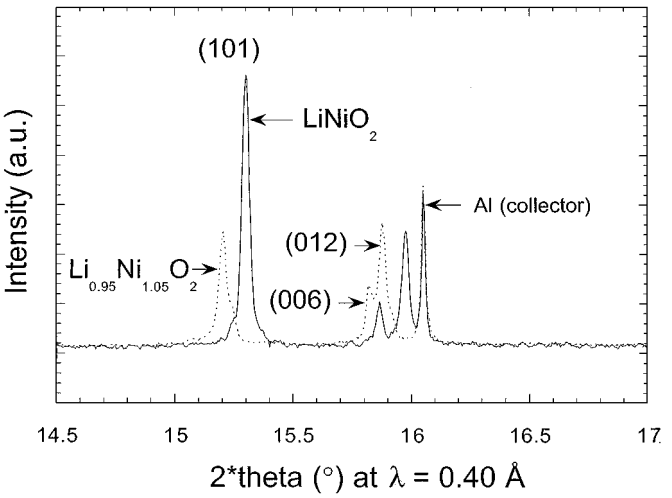

FIG. 1. Synchrotron X-ray powder diffraction patterns of $LiNiO_2$ and $Li_{1-x}Ni_{1+x}O_2$ ($x = 0.058$); only the 2θ range used to deduce the value of x is displayed (see text).

The plastic electrode laminates were prepared as previously described (9) by mixing in an acetone solution the electrochemically active materials ($LiNiO_2$ or $LiCoO_2$ for the positive, graphite MCMB-2528 (Osaka Gas) for the negative), SP carbon black, PVDF-HFP copolymer matrix (Elf-Atochem), and dibuthyl-phtalate plasticizer (DBP) 4N (Aldrich). The resulting paste was then used to produce plastic electrode films (65% weight loaded with active material) by solvent casting. Free standing separator films were made by mixing an inorganic filler such as SiO_2 with PVDF-HFP/plasticizer (DBP) solutions in acetone, and then by casting the solution. These independent plastic laminated tapes were cut in $5 \times 4\ cm^2$ squares to produce our standard size plastic batteries. The DBP plasticizer was extracted using ether. The resulting DBP-free laminates were dried under vacuum for a few hours prior to entrance into a dry box. The 3-electrode Li-ion plastic cells consist of

TABLE 1

	a (Å)	b (Å)	c (Å)	β (°)	γ (°)	V (Å^3)	Z
$LiCoO_2$	2.8037(1)	2.8037(1)	13.9893(2)	90	120	95.23	3
$LiNi_{0.7}Co_{0.3}O_2$	2.8498(1)	2.8498(1)	14.0946(5)	90	120	99.13	3
$LiNiO_2$	2.8623(1)	2.8623(1)	14.1134(5)	90	120	100.28	3
$Li_{0.95}Ni_{1.05}O_2$	2.8806(1)	2.8806(1)	14.1664(3)	90	120	101.80	3
CoO_2	2.8048(1)	2.8048(1)	4.2509(5)	90	120	29.31	1
	2.8208(1)	2.8208(1)	4.2403(3)	90	120	29.72	1
NiO_2	4.8754(3)	2.8141(2)	5.5820(3)	125.836(4)	90	62.09	2
$Ni_{1.05}O_2$	4.863(3)	2.8027(9)	5.582(3)	126.09(2)	90	61.48	2

the stacking of six components: a copper grid as current collector, a carbon-based negative electrode, two plastic electrolyte separators (between which the reference electrode is placed), a positive electrode, and an aluminum grid current collector. They were assembled in a dry box using an electrolyte solution (1 M $LiPF_6$ in EC-DMC (2:1)) as plasticizer. The battery laminates (0.5 mm thick) were then sealed in aluminum-metallized plastic bags (e.g., coffee bags).

The resulting 3-electrode plastic batteries were placed on the BM16 diffractometer at ESRF in transmission geometry, using a rotating sample holder to limit preferential orientation effects. Rotation was limited to $\pm 90^\circ$ due to the connecting wires allowing electrochemical and temperature control of the cell *in situ*, while recording the XRD patterns. For high-temperature measurements, two heating tape elements were placed on each side of the plastic bag, with a thermocouple, keeping the X-ray beam passage uncovered; the Al-coated plastic bag of the cell has a good enough thermal conductivity to ensure a homogeneous temperature.

Electrochemical tests were controlled using a Mac-Pile system (Bio-Logic, Claix, France). The cells were submitted to a variety of cycling or resting periods by usually limiting the positive-to-reference electrode potential, unless otherwise specified. Cycling tests were carried out in either galvanostatic or potentiostatic mode depending on the type of study, as will be specified in the text. For all *in situ* measurements, very low charging/discharging rates were used in order to be close to equilibrium conditions. For each study, two cells, one of which was placed on the synchrotron beam line, were cycled in parallel.

For $LiCoO_2$, cells were charged to 5.2 V, then maintained at this potential for the time needed to obtain a series of 10 superimposable X-ray patterns. When dealing with such highly oxydized materials, caution must be exercized in performing structural studies. Maintaining the cell at constant voltage during the X-ray collection is a requirement due to the continuous self-discharge that, if not compensated, will lead to multiphase materials. This explains why *ex situ* X-ray measurements on the $(Ni, Co)O_2$ members and especially CoO_2, are practically impossible since once the cell is disconnected, the active material (e.g., $(Ni, Co)O_2$) will be slightly reduced ($Li_x(Ni,Co)O_2$) and not representative of the fully delithiated material.

The effect of temperature was investigated by heating cells at 80°C, and placing them intermittently on the beam line for diffraction pattern acquisition. Because of beam allocation time limits, these high-temperature experiments could not be pursued beyond 8 days.

The diffraction data have been collected using the nine-channel crystal analyzer stage developed for the ESRF BM16 beamline to provide excellent resolution with good statistics. The 2θ (0 to 80°) angular range, using $\lambda = 0.65$ Å for NiO_2 and $\lambda = 0.40$ Å for CoO_2, was scanned in about 10 minutes. Data from each analyzer were scaled and added, and the data from each scan could be added. When x was equal to 0 (e.g., NiO_2, CoO_2), all similar patterns were added to improve the statistics. Cell parameters were refined using the pattern matching option of the profile fitting program FullProf (13) with pseudo-Voigt profile functions. Fullprof is a code based on the Rietveld method of full profile refinement of a powder diffraction pattern. This code can be used in two ways that are (1) whole-pattern fitting (cell constrained refinement) and (2) profile fitting structure refinement (Rietveld refinement). We used the whole-pattern fitting approach that consists in analyzing the overall profile without reference to any structural model. Only cell and profile shape parameters are refined, and the integrated intensities are calculated by iteration. This approach is very convenient to extract a full set of integrated "observed" intensities to be fed in direct method codes, in order to find a correct starting structural model to be refined.

RESULTS

The Li_xNiO_2 System

Due to the large amount of *in situ* and *ex situ* work (14, 15) already performed on the Li_xNiO_2 system over a broad range of x values, we only focused on materials with $x < 0.1$ and on solving the structure of Li_0NiO_2. The charging conditions for the $LiNiO_2$/C cell used are shown in Fig. 2.

The final deintercalation for the *in situ* XRD study was performed on a compound previously galvanostatically deintercalated to a nominal $x = 0.25$ for 16 h and kept for 3 days in open circuit during which the potential equilibrated to 4.0 V with a final drift lower than 0.7 mV/h. Oxidation was then carried out in potential-controlled mode from the 4.0 V equilibrium, with 5 mV steps and a minimum 15 mA current (for a sample mass of 515 mg). At 4.25 V, the potential was maintained constant for 20 h and the current decreased from 30 to 0.65(5) mA/g (i.e., close to a C/400 equivalent rate) and then stabilized within about 7 h at this value. The nominal x value was then close to -0.05 (Fig. 2). The 0.65 mA/g steady current (e.g., current needed to compensate for the cell self-discharge) is responsible for the negative x values obtained. Assuming that the nominal $x = -0.05$ reached when the oxidation current stabilized corresponds in fact to $x = 0$, we deduce an actual x value at the beginning of the potentiodynamic oxidation close to 0.30. This is in agreement with the fact that the initial equilibrated OCV of 4.0 V corresponds to that of the monoclinic/second hexagonal phase equilibrium, which is in the 0.28–0.38 x range (16, 17).

In situ XRD patterns were continuously collected during the potentiodynamic oxidation of the cell. The powder pattern for NiO_2, obtained after the cell was placed on floating

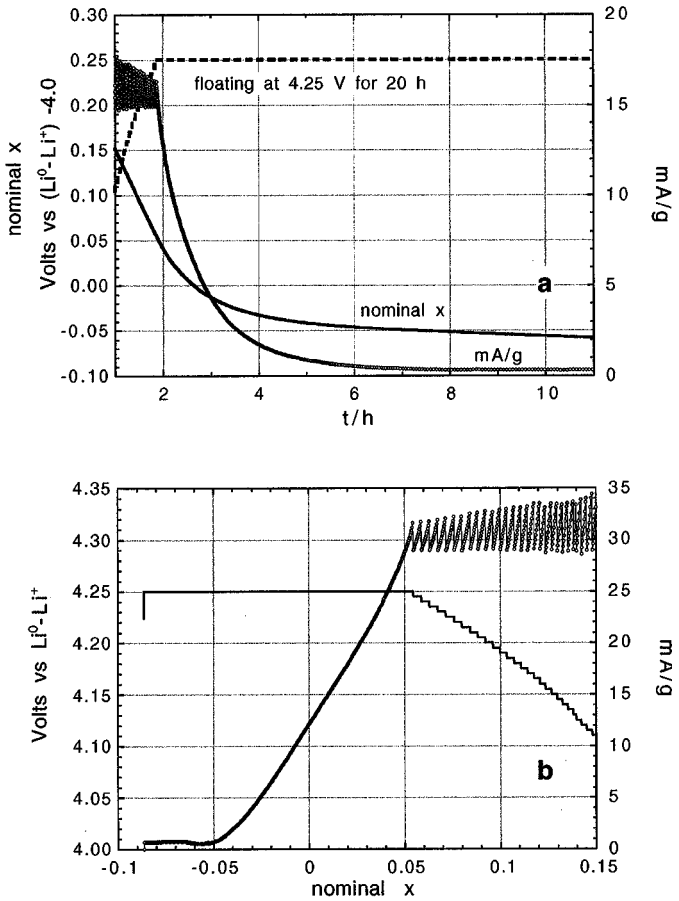

FIG. 2. Electrochemical conditions of *in situ* final deintercalation of $LiNiO_2$: evolution of the oxidation current (open dots) and potential (full line) during oxidation as a function of time (a) and of nominal lithium content x (b). Potentiodynamic oxidation was carried out using 5 mV potential steps from an equilibrated initial state at 4.0 V (x[nominal] = 0.253) with minimum current 0.39 mA/g, up to 4.25 V; this potential was then maintained for 20 h.

at 4.25 V for 20 h ($x = -0.08$ and $I = 0.65$ mA/g on Fig. 2) is shown in Fig. 3. The NiO_2 unit cell was determined using DICVOL (18). Only one solution in monoclinic symmetry was found. The indexation of the lines clearly shows that only three space groups are consistent with the observed extinctions: $C2/m$, Cm or $C2$. The final refinement led us to the centric group $C2/m$ as the solution. Cell parameters were refined in pattern matching mode using FullProf, and led to the following parameters: $a = 4.8754(3)$ Å, $b = 2.8141(2)$ Å, $c = 5.5820(3)$ Å, $\beta = 125.836(4)^\circ$. $Z = 2$ has been determined from the estimated density of NiO_2. At the same time, integrated intensities were extracted, and direct methods were performed using SIRPOW92 (19).

The structural model proposed consisted in $C2/m$ (No. 12) space group, with Ni at position 0 0 0 (2*a*) and oxygen at x 0 z (4*i*) with $x = 0.493(4)$ and $z = 0.231(2)$. The refinement showed two remaining problems: (i) asymmetry in low-angle reflections, due to the axial divergence of the beam, which was corrected using a modified pseudo-voigt function in FullProf, (ii) the presence of a few broader NiO_2 reflections. The latter was solved by introducing two identical phases with different Cagliotti polynoms in the refinement. This led to a better profile description ($R_{wp} = 13.8\%$) and to a structure reliability factor $R_B = 7.7\%$. Finally, site occupancies were refined, and a perfect stoichiometry for NiO_2 was achieved. Final results are given in Table 2. The structure of NiO_2 is a distorted CdI_2 structure (Fig. 4).

The $Li_xNi_{0.7}Co_{0.3}O_2$ System

X-ray powder patterns were collected on a $Li_xNi_{0.7}Co_{0.3}O_2$/C Li-ion cell that was galvanostatically charged to 4.5 V and fitted on the basis of an hexagonal unit cell (Fig. 5). Note, that the c axis increases slightly from 14.1 ($x = 1$) to 14.35 Å ($x = 0.5$) before dropping to 12.625 Å for $x = 0$, while the a axis decreases continuously from 2.8948(1) to 2.8735(1) Å over the same x range. Such an evolution of the cell parameters upon Li removal is similar to that previously established from X-ray for Li_xNiO_2 ($0 < x < 1$).

The Li_xCoO_2 System

We performed *in situ* XRD study on several 3-electrode Li_xCoO_2/C plastic cells made from the same electrode preparation. For studying the end member, synchrotron XRD patterns were collected as for the Li_xNiO_2 system: the cell was first galvanostatically charged to $x = 0.5$ at C/20 rate and equilibrated in open circuit for several days, then charged under potentiodynamic control (mainly at 20 mV/0.2 h steps) up to 5.2 V, and finally maintained at this potential (Fig. 6a). One can see the increase in the deintercalation current around 4.6 V, in agreement with previous observations on incremental capacity voltammograms (Fig. 6b), and a new increase in the current from 4.8 V to the 5.2 V end potential. At that point, the current decreased from 12 to 6 mA/g for 1 h, and then became very noisy. For the same reasons as in the Li_xNiO_2 case (e.g., parasitic currents), the nominal compositions (x) reach negative values. The XRD pattern of the CoO_2 end member was recorded after an 11-h equilibration at 5.2 V. While always maintaining this potential, the cell was then removed from the beam for 8 h, then its XRD pattern remeasured *in situ* for 6 h, in order to check for possible further structural evolution. No changes were observed.

The X-ray powder patterns (Fig. 7) were fitted on the basis of a hexagonal unit cell, and the variation of the a and c parameters are shown in Fig. 8 together with those previously reported by Amatucci *et al.* (6) for comparison. While there is an agreement over the general trend, a subtle

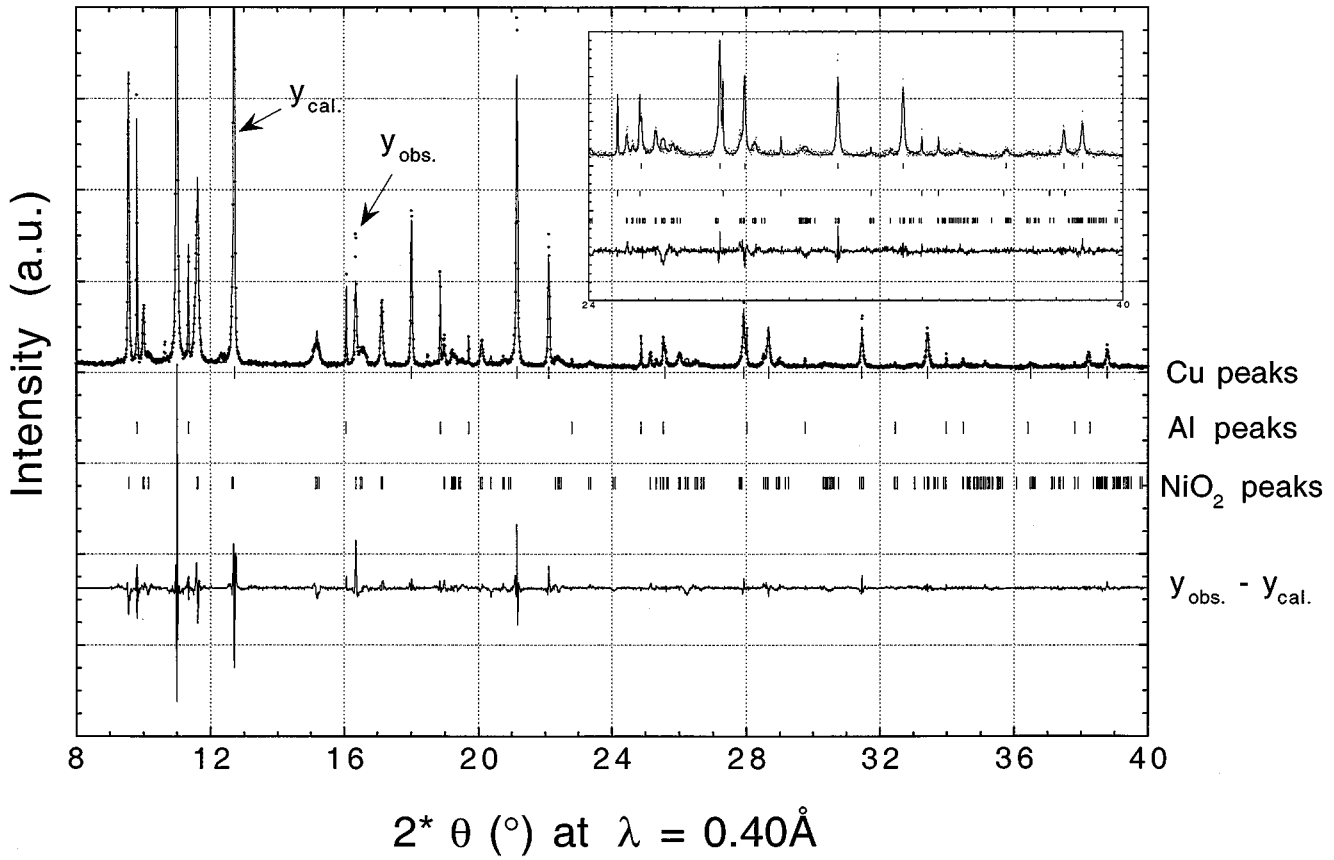

FIG. 3. Synchrotron X-ray powder pattern of the NiO_2 end member. The difference I_{obs}–I_{calc} is shown at bottom.

difference can be noted, namely in the phase sequence encountered upon Li removal. Indeed, the monoclinic distortion near $x = 0.2$ previously observed (6) could not be confirmed from our synchrotron data. Dahn *et al.* (20) have shown that for $LiCoO_2$ a small amount of 3d-metal doping (Ni) is sufficient to strongly modify the room temperature Li-phase diagram. Although these two samples appear identical from both X-ray and atomic absorption data, they are not issued from the same batch, and could well differ in the amount of doping impurities, thereby accounting for the observed difference on the basis of Dahn's finding.

TABLE 2
Final Results for NiO_2

Space group cell parameters (Å)	Atom	Site	x	y	z	B_{iso} (Å^2)
$C2/m$ $z = 2$						
$a = 4.8754(3)$	Ni	2*a*	0	0	0	0.92(2)
$b = 2.8141(2)$						
$c = 5.5820(3)$	O	4*i*	0.493(4)	0	0.231(2)	0.94(3)
$\beta = 125.836(4)^\circ$						

Note. $R_{wp} = 13.8\%$; $R_{Bragg} = 7.7\%$; 190 NiO_2 reflections used in the refinement.

For the fully delithiated CoO_2 sample, an analytical treatment of the collected X-ray data similar to the one carried out for NiO_2 was first performed (21), but a complete structural determination could not be achieved. An average hexagonal cell was obtained assuming that each observed diffraction peak consists of only one reflection to provide the points reported on Fig. 8. Note that the value of *a* for Li_xCoO_2, $x = 0$ (white dot on the curve) differs from that previously reported by Amatucci *et al.* (6). At first a refinement of this pattern in the cell-matching mode enables a fairly good description of the CoO_2 phase in monoclinic symmetry ($R_{wp} = 10.8\%$), with the following cell parameters: $a = 4.8413(3)$ Å, $b = 2.8031(1)$ Å, $c = 12.7474(3)$ Å, $\beta = 90.10(1)^\circ$ (21). In order to shed some light on this disagreement, a second acquisition run with better statistics in amplitude was carried out. The main result is that the diffraction lines, that at first glance appeared as single reflections, actually consist of two sets of lines. A better pattern matching ($R_{wp} = 9.5\%$) of the CoO_2 end member was then

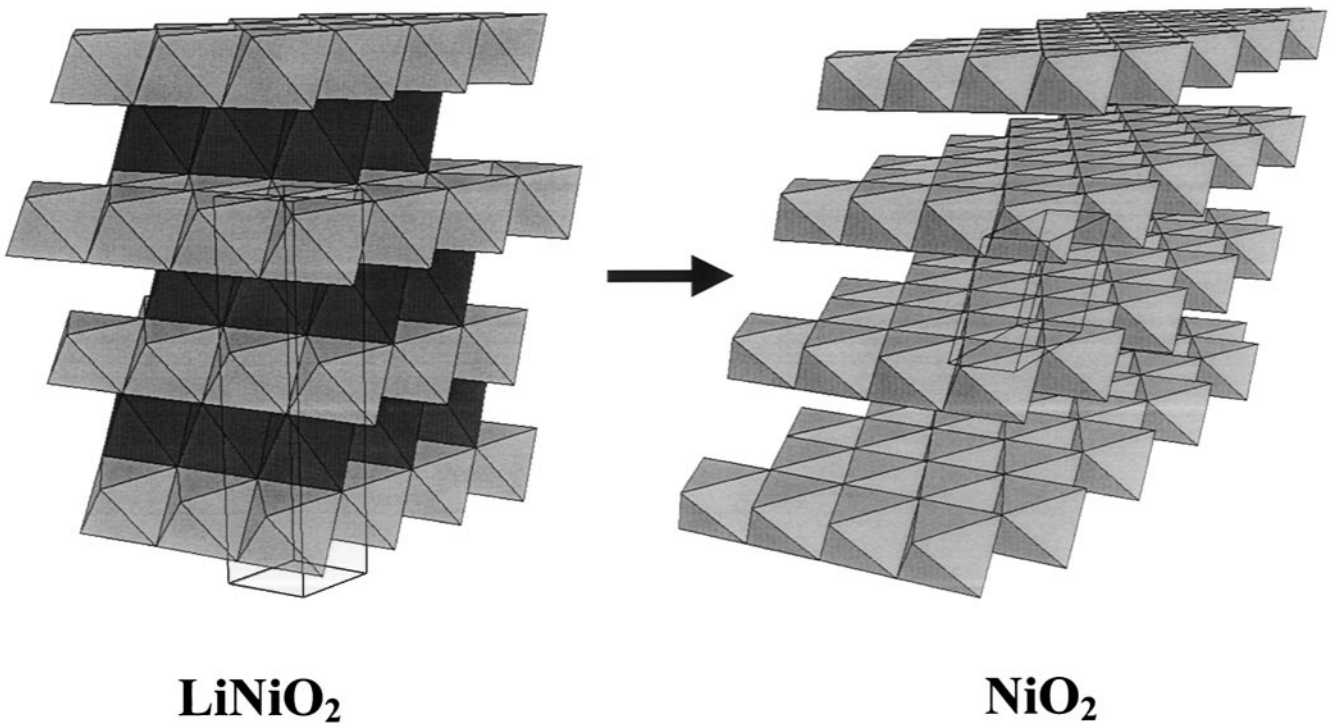

FIG. 4. Structures of $LiNiO_2$ and of the end member NiO_2, based on a three-dimensional packing of octahedral sheets. The basic unit cell is drawn for both structures, to emphasize the monoclinic distortion upon Li removal.

obtained by assuming the coexistence within the sample of two CdI_2-type phases (Fig. 9):

— a major phase A (70%) with broad reflection (WHM in $2\theta = 0.088°$): it turns out to be an oxygen-deficient phase ($CoO_{1.92}$), with hexagonal lattice parameters $a =$ 2.8049(2) Å and $c = 4.2522(6)$ Å, and

— a minor phase B (30%), stoichiometric in oxygen, with narrow diffraction peaks (WHM in $2\theta = 0.038°$) and hexagonal lattice parameters $a = 2.8221(2)$ Å and $c =$ 4.2296(6) Å.

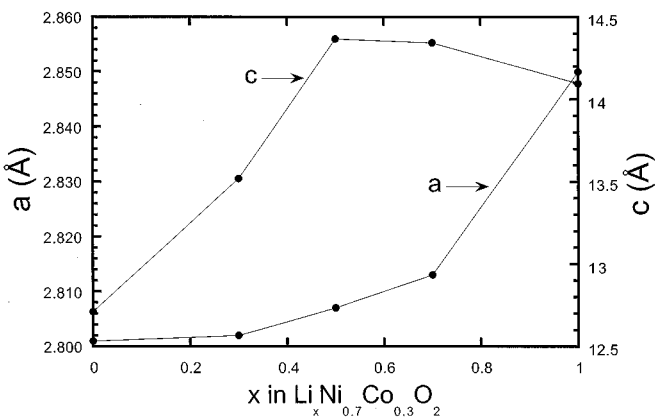

FIG. 5. Variation of *a* and *c* lattice parameters during electrochemical lithium extraction from $LiNi_{0.7}Co_{0.3}O_2$, as determined by *in situ* transmission X-ray diffraction.

The positions of cobalt and oxygen atoms in these phases have been determined from the cadmium iodide model structure (space group *P*-3*m*1), with cobalt in the (1*a*) special position (Table 3). The location of oxygen is more problematic because the refinement poorly converges. This could be due either to the high overlapping of the diffraction lines, making the determination of integrated intensities very difficult, or to a local disorder of oxygen atoms, so that the observed structure is an average structure. Such difficulties precluded the exact determination of the oxygen atoms position. For both CdI_2-type phases, however, the refinements consistently give reduced distances (as short as 2.20 Å for phase B) between neighboring oxygen atoms belonging to layers parallel to the *a*, *b* plane, indicating possible O–O bonding in the structure.

It is interesting to note that among the CdI_2-type phases presently reported to describe the end member CoO_2, one has the same *a* and *c* axis as those reported by Amatucci *et al.* (6). The main difference lies in the presence of another phase of similar structure, but having oxygen vacancies. These vacancies, introduce disorder within the oxygen network, explaining why the diffractions lines are wider for phase A than B. Based on the Gao *et al.* (22) work showing evidence for oxygen removal within the spinel framework upon charging an $LiMn_2O_4$/Elec./C cell, the possibility of creating oxygen vacancies in $LiCoO_2$ at high charging voltage is quite likely. Furthermore, although oxygen vacancies,

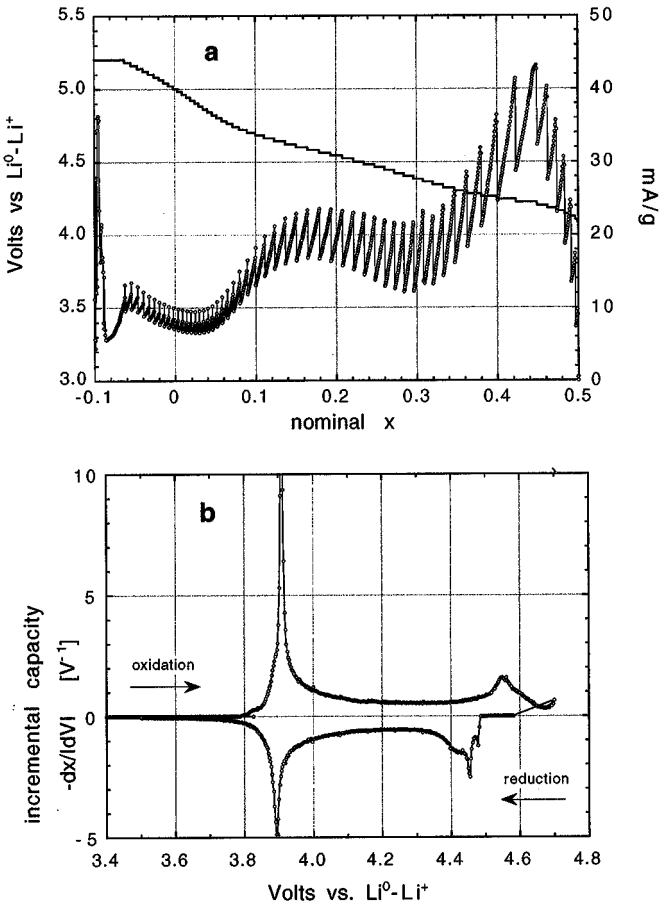

FIG. 6. Electrochemical conditions of *in situ* final deintercalation of $LiCoO_2$: (a) evolution of the oxidation current (open dots) and potential (full line) during the oxidation as a function of the nominal lithium content. Potentiodynamic oxidation was carried out using 20 mV/0.2 h steps from an equilibrated initial state at 4.08 V (x[nominal] = 0.5) up to 5.2 V; this potential was then maintained for 38 h. (b) Electrochemical step-potential spectroscopy plot of Li_xCoO_2.

to our knowledge, have never been reported for $LiCoO_2$, Na_xCoO_2-δ phases are known to prone to oxygen vacancies (23).

The experimental factors leading to the coexistence of two different phases in CoO_2 remain an open question: does the A/B ratio depend on the synthesis conditions of $LiCoO_2$ precursor, or on the cell charge conditions? Further work dealing with this issue is planned during our next run at ESRF.

Thermal Stability of Fully Charged $Li_yNi_{1-x}Co_xO_2$ Electrodes

$Li_yNi_{1-x}Co_xO_2$/C cells were galvanostatically charged at room temperature up to 4.5 V, then maintained at this potential while their temperature was raised to 80°C. The batteries were then placed intermittently on the synchrotron beam-line for data collection. The X-ray powder patterns of two fully-charged cells $x = 0$ (e.g., NiO_2) and $x = 0.3$ ($Ni_{1-x}Co_xO_2$) stored for 8 h at 80°C are displayed in Fig. 10 together with the X-ray powder pattern obtained for a room temperature fully-charged $LiNiO_2$/C cell. They clearly show that a 80°C temperature induces a rapid evolution of the powder patterns with the appearance and rapid growth of extra Bragg peaks corresponding to NiO. The amplitude of the NiO extra peaks, or its intensity ratio with respect to the NiO_2 [101] Bragg peak is larger for the $x = 0$ electrode than for the Co-substituted one ($x = 0.3$). After 3 days at that temperature, Bragg peaks corresponding to the precursor $Ni_{1-x}Co_xO_2$ phases were barely detectable. A temperature-induced decomposition was also noted for the fully charged $Li_{1.05}Ni_{0.95}O_2$ stored 8 h at 80°C, and, based on the intensity of the NiO bragg peaks, it appeared that this phase decomposition occured at a similar rate as for a fully charged $LiNiO_2$/C cell.

DISCUSSION

We have reported the structural determination and thermal stability of the electrochemically delithiated $Li_xNi_{1-x}Co_xO_2$, with special attention to the $Ni_{1-x}Co_xO_2$ end members ($x = 0$ and 1). Both metastable phases maintained the CdI_2-type layered structure. NiO_2 crystallized in a monoclinic basic unit cell, while the CoO_2 end member can be described with the coexistence of two CdI_2-type structures.

The proposed distorted CdI_2-structure ($C2/m$) for the NiO_2 end member differs from the $CdCl_2$-type structures (R-3m) previously reported (6, 14). The origin of these structural differences roots on the well known fact, that $LiNiO_2$ precursors, depending on the synthesis conditions, can have various degrees of cationic mixing in the Li layers. The presence of Ni within the Li layer governs the gliding of the NiO_2 layers necessary in going from a $CdCl_2$ to a CdI_2-type structure, thereby accounting for the various reported structures for the NiO_2 end member. For stability reasons, the Van der Waals gap must be completely devoid of cationic species to accommodate the $CdCl_2$–CdI_2 transformation. Cationic occupation of the Van der Waals gap in the CdI_2 phase would necessitate face sharing cationic octahedral in the opposing planes, which is unstable. This instability was directly evidenced by Glen *et al.* (6) showing that once ε lithium is reintercalated into the CoO_2 CdI_2-type oxide structure, there is an immediate formation of a $CdCl_2$ second phase. The observed distorted CdI_2-type structure presently observed for NiO_2 and not purely CdI_2 as for CoO_2, may simply be explained by the presence of Ni ions in the interslab space, minimizing the lattice instability so that there is a distortion of the CdI_2 cell. Thus a pure CdI_2-structure could well exist in Ni-free interslab NiO_2. The

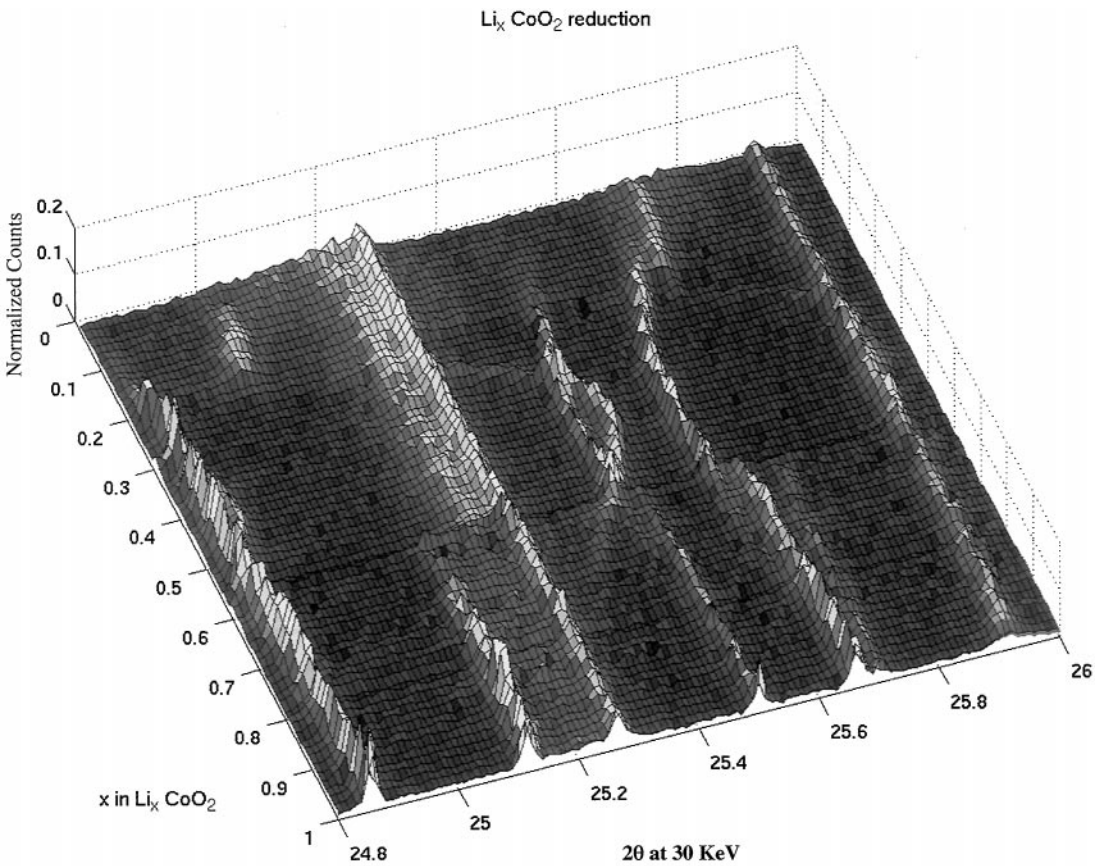

FIG. 7. Evolution of a typical part of the synchrotron X-ray diffraction patterns collected *in situ* on a Li_xCoO_2 battery during Li deintercalation.

basis for this instability does not exist within the $LiCoO_2$ system for which cationic mixing of Co within the Li layers was never experimentally observed consistent with the greater ionic radii difference between Li^+ and Co^{3+} than between Li^+ and Ni^{+3}.

The existence of such materials, based on the large repulsion between the highly negative charged MO_2 layers in the absence of cation within the Van der Waals gap, is somewhat surprising. Layered oxides with tetravalent cations are not common, as witnessed from the numerous worldwide attempts to prepare, without success, the equivalent Fe- and Mn-based layered oxides. The layered Ni and Co hydroxides $Ni(OH)_2$ and $Co(OH)_2$ constitute another very instructive example where Ni and Co cations can partially oxidize to a $+4$ state. Proton can be electrochemically deintercalated from these phases to produce first the oxyhydroxide β-HMO_2 with M^{+3} cations, and upon further oxidation γ-$H_{1-x}MO_2$ phases containing large amounts of M^{+4} ions.The proton deintercalated γ-phase forms more easily for $M = Ni$; in fact, γ-$H_{1-x}CoO_2$ can only be obtained under harsh oxidizing conditions, and the amount of Co^{+4} in it never exceeds 20% (24, 25). This is consistent with the present study showing that NiO_2 is obtained at a lower oxidizing potential than CoO_2; i.e., the latter is more difficult to prepare.

Despite this comparison and several tentative explanations (for instance ferromagnetic distortion leading to a corrugated CoO_2 layer), the question why the stable NiO_2 and more so CoO_2 phases form remains. A clue is supplied by an analysis of the bonding distances deduced from structural refinement. Surprisingly, some of the oxygen–oxygen interplanar anion distances come out shorter than normally expected. Such a shortening is by no means fortuitous, but most likely indicative of an electronic transfer from anionic to *d*-cationic levels. Chemically speaking, this means that the metal cation is becoming more electronegative than oxygen, so that holes will appear on the oxygen. A similar situation, as determined by EELS measurements, was recently shown to occur with the high T_c cuprates having holes on the oxygen anion (26). While relatively rare among oxides, such an anion–cation redox chemistry is quite common with chalcogenides, as pioneered by J. Rouxel as early as 1975 when dealing with $NbSe_3$, and then further developed until its last days to account for the redox chemistry

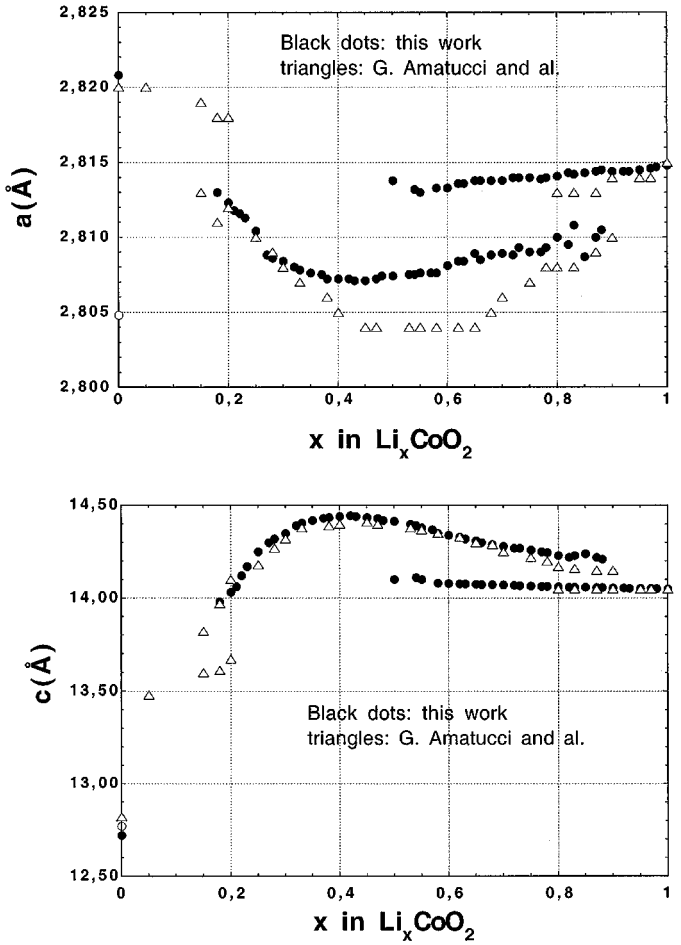

FIG. 8. Variation of a and c lattice parameters during electrochemical lithium extraction from $LiCoO_2$, as determined by *in situ* transmission X-ray diffraction, compared with results previously obtained (Ref. 6). White dots correspond to the oxygen-deficient $CoO_{2-\delta}$ phase (see text).

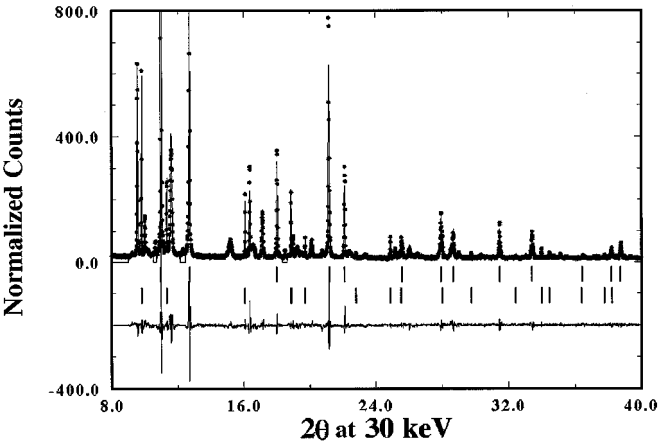

FIG. 9. Synchrotron X-ray powder pattern of the CoO_2 end member obtained *in situ* on a Li_xCoO_2/C cell maintained 10 h at 5.2 V. The difference I_{obs}–I_{calc} is shown at the bottom.

in the chalcogenides, and to explain the ability to obtain new phases by Chimie Douce (27–30).

Briefly, a *d–sp* redox process occurs when the respective positions of the anionic antibonding *sp* levels and cationic *d* levels lie at similar energies. Such a situation is favored with lowering the anionic electronegativity (e.g., going from O to S, Se, and Te) and thereby frequently encountered with the heavier chalcogenides, rather than with oxides. On oxidation, the *d–sp* redox competition corresponds to a partial filling of the *d* cationic levels and simultaneous depopulation of the top of an *sp* anionic band having an important antibonding character, which could result in a shortening of the anion–anion separation.

On the other hand, the lithium extraction reaction from $LiCoO_2$ to form layered CoO_2 implies an oxidation of the Co^{+3} level situated about the *sp* antibonding level of the anion to Co^{+4} having a *d* level falling within the *sp* anionic band. Apparently such a process could occur without involving the oxidation of O^{2-}. However, it should be realized, as previously reported (31), that upon oxidation there is always a small quantity of Co going into solution so that the formula is most likely $Li_xCo_{1-y}O_2$. Thus, once all the $(1-y)$ Co^{+3} are oxidized (e.g., once $1-y$ lithium has been removed) for the intercalation to further proceed leading to a complete Li removal as experimentally observed, an extra $x = 4y$ electrons $(x + 4(1-y) = 4 \rightarrow x = 4y)$ are needed. Such extra electrons can only be provided by the following oxidation reaction

$$4yO^{2-} \rightarrow 2y(O_2)^{2-} + 4ye^-$$

Thus the overall reaction will occur in two steps:

(1) $LiCoO_2 \rightarrow Li_xCo_{1-y}O_2$

(2) $Li_xCo_{1-y}O_2 \rightarrow Co_{1-y}O_{2-4y}^{2-}(O_2)_{2y}^{2-}$

The depopulation of the top of the *sp* band, which has an important antibonding character, results in a shortening of the anion–anion separation as observed leading to a "3d-

TABLE 3
Final Results for CoO_2

Space group cell parameters (Å)		Atom	Site	x	y	z	B_{iso} (Å^2)
P-3*m*1	$Z = 1$						
Phase A	Phase B	Co	1a	0	0	0	0.45(4)
$a = 2.8048(1)$	$a = 2.8208(1)$						
$c = 4.2509(5)$	$c = 4.2403(3)$	O	2*d*	$\frac{1}{3}$	$\frac{2}{3}$	$0.17 < z < 0.23$	0.70(7)

Note. Pattern matching mode: $R_{wp} = 9.5\%$.

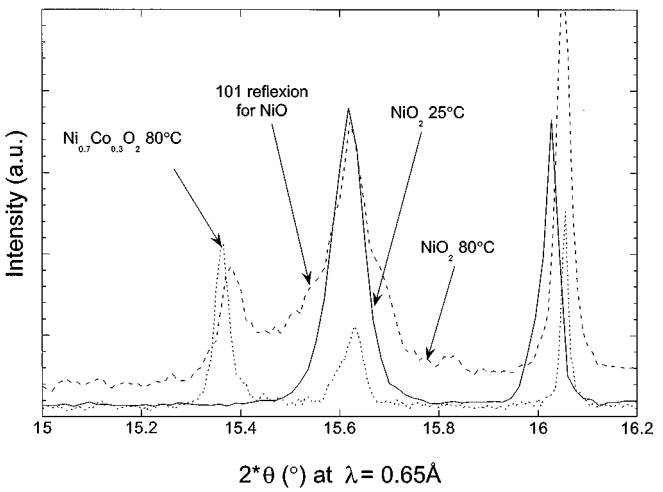

FIG. 10. *In situ* synchrotron X-ray powder patterns of $LiNiO_2$/C and $LiNi_{0.7}Co_{0.3}O_2$ cells stored at 80°C at constant potential 4.5 V for 18 h. The Bragg peak located at $2\theta = 15.7$ indicates the presence of NiO.

type polymerization" that could then account for the stability of the CoO_2 phase. This scenario is similar to the one previously found for the Li extraction from Li_2FeS_2, which consists in the two following steps: (1) oxidation of Fe^{+2} to Fe^{+3}, (2) formation of anionic pairs. Both cations and anions are successively oxidized leading to a new FeS_2, which can be written as $Fe^{3+}(S_2^{2-})_{0.5}S^{2-}$ with a partial degree of out-of-plane S–S bonding.

The above picture, which could appear to be hand-waving to nonchemists, was recently theoretically settled by Ceder *et al.* (32, 33). Applying first-principles method calculations to the Li_xCoO_2 system, the authors showed that the intercalation potential can be tailored through modifications of charge exchange with oxygen. Their result can be understood in terms of hybridization of the metal–oxygen orbitals, and more specifically as a redistribution of the molecular orbital between the Co and oxygen atomic orbitals during the reversible Li removal/uptake process.

Finally, regarding phase stability, our thermal study has shown that fully charged ($Ni_{1-x}Co_xO_2$) electrodes decompose at temperatures as low as 80°C in nonaqueous electrolyte. So, without any doubt, these phases are not in thermodynamically ground states (e.g., they are metastable), although they can be produced by electrochemical delithiation. This unstability is at the origin of the safety hazards encountered with $LiNiO_2$ and $LiCoO_2$ when extending their state of charge (e.g. delithiation). Perhaps coincidentally, most engineering materials are actually metastable and not thermodynamically stable.

Chemistry can be used to enhance materials thermodynamic stability to ensure their safe implementation in practical batteries. To capitalize on the great advantage of $LiNiO_2$, researchers have added cobalt ($LiNi_{1-x}Co_xO_2$) (34) and aluminum while maintaining Co substitution ($LiNi_{1-x-y}Co_xAl_yO_2$) (35, 36). Besides their enhanced electrochemical performance, the present study has shown that, at 80°C in $LiPF_6$-EC-DMC electrolyte, the Co-substituted NiO_2 phases are more resistant toward decomposition than the nonsubstituted ones (e.g., they are slightly safer to use), in agreement with previously reported differential scanning calorimetry (DSC) results (37). Similar thermal structural stability experiments are presently being pursued for $LiNi_{1-x}Co_xO_2$/C cells as a function of their state of charge. Finally, there have been recent reports claiming that two- or threefold cationic substituted $LiNiO_2$ phases ($LiNi_{1-x}Ti_{x/2}Mg_{x/2}O_2$ or $LiNi_{1-x-y}Ti_{x/2}Mg_{x/2}Co_yO_2$) (38) are highly resistant against thermal decomposition as deduced by DSC. Knowing how these cationic substitutions will affect the anion–cation redox chemistry in such materials should be of great interest.

CONCLUSION

The refinement of NiO_2 structure has been successfully performed. NiO_2 is stoichiometric and adopts a distorted CdI_2 structure. The refinement of CoO_2 structure was more problematic. Two slightly different CdI_2-type structures corresponding to stoichiometric (CoO_2) and oxygen nonstoichiometric ($CoO_{1.92}$) were needed to refine the X-ray data. Cobalt atoms positions have been determined, but the position of the oxygen atoms, because of local disorder, could not be determined accurately, while strongly pointing toward the presence of shortened O–O bond distances. Further structural work is required to strengthen this point, as well as to address the issue whether or not the ratio of $CoO_{1.92}$ and CoO_2 phases depends on the synthesis conditions of the $LiCoO_{2-\delta}$ precursor or on the cell floating time at 5.2 V. Finally, we showed that Co doping minimizes the thermal decomposition of $LiNi_{1-x}Co_xO_2$. However, additional experiments are needed to ensure that the origin of this observation lies in the real difference between the thermodynamic stability of the samples rather than in their decomposition rates.

ACKNOWLEDGMENTS

The authors want to thank A. Delahaye and A. Rougier for technical discussions.

REFERENCES

1. M. Figlarz *in* 'Soft Chemistry Routes to New Solids," Materials Science Forum, Trans. Tech. Publications, Vol. 152, p. 55, 1994.
2. J. Rouxel, "Advances in the Synthesis and Reactivity of Solids," Vol. 2, p. 27, 1977.
3. T. Nagaura, "4th International Rechargeable Battery Seminar," Deerfield Beach, Florida 1990.
4. T. Ohzuku and A. Ueda, *Solid State Ionics* **69,** 201 (1994).

5. J. N. Reimers and J. R. Dahn, *J. Electrochem. Soc.* **139,** 2091 (1992).
6. G. G. Amatucci, J-M. Tarascon, and L. C. Klein, *J. Electrochem. Soc.* **143,** 1114 (1996).
7. J. R. Dahn, M. Py, and R. Haering, *Can. J. Phys.* **60,** 307 (1982).
8. J. M. Tarascon, G. W. Hull, P. Marsh, and Ter Haar, *J. Solid State Chem.* **66,** 204 (1987).
9. J-M. Tarascon, A. S. Gozdz, C. Schmutz, F. Shokoohi, and P. C. Warren, *Solid State Ionics* **86,** 49 (1996).
10. U.S. Patent 5,425,932 Bell Communications Research, Inc., (1995).
11. A. Rougier, P. Graveneau, C. Delmas, *J. Electrochem. Soc.* **143,** 1168 (1996).
12. N. Reimers, J. R. Dahn, J. E. Greedan, C. V. Stager, G. Liu, I. Davidson, U. von Sacken, *J. Solid State Chem.* **102,** 542 (1993).
13. J. Rodriguez Carvajal in "Collected Abstracts of Powder Diffraction Meeting. Toulouse, France, July 1990" p. 127.
14. T. Ohzuku, A. Ueda, and M. Nagayama, *J. Electrochem. Soc.* **140,** 7 (1993).
15. J. R. Dahn, U. von Sacken, C. A. Michal, *Solid State Ionics* **44,** 87 (1990) provides verification.
16. Lee *et al. Solid State Ionics.* **67,** 123 (1993).
17. Barker *et al., Solid State Ionics.* **89,** 25 (1996).
18. A. Boultif and D. Louër, *J. Appl. Crystallogr.* **24,** 987 (1991).
19. C. Giacovazzo, *Acta Cryst. A* **39,** 685 (1983).
20. J. N. Reimers, J. R. Dahn, and Y. von Sacken, *J. Electrochem. Soc.* **140,** 2753, (1993).
21. L. Seguin, G. Amatucci, M. Anne, Y. Chabre, P. Strobel, J. M. Tarascon, and G. Vaughan, *J. Power Sources*, In press.
22. Y. Gao, J. R. Dahn, *J. Electrochem. Soc.* **143,** 100 (1996).
23. C. Delmas, J. J. Braconnier, C. Fouassier, and P. Hagenmuller, *Solid State Ionics* **3/4,** 209 (1981).
24. N. Sac-Epée, M. R. Palacin, B. Beaudoin, A. Delahaye-Vidal, T. Jamin, Y. Chabre, and J-M Tarascon, *J. Electrochem. Soc.* **144,** 3896, (1997).
25. A. Delahaye-Vidal, N. Sac-Epée, F. Portemer, B. Beaudoin, B. Beaudoin, M. Figlarz, and T. Jamin, *in* "Proceeding Solid State Ionics IV" (G. A. Nazri and J-M. Tarascon, M. Schreiber, Eds.), Vol. 9, p. 107, Materials Research Soc. Pittsburgh, 1995.
26. D. D. Sarma, *in* 'Chemistry of High Temperature Super-Conductors" (C. N. Rao, Ed.), p. 348, World Scientific Singapore, 1991.
27. J. Rouxel, *in* "Design and Chemical Reactivity of Low Dimensional Solids," *Supramolecular Architecture*, p. 88, Amer. Chem. Soc. 1992.
28. J. Rouxel, *Curr. Sci.* **173,** 31 (1997).
29. J. Rouxel, *Mol. Crist. Liq. Cryst.* **310,** 1 (1998).
30. J. Rouxel, *Chem. Eur. J.* **9,** 1053 (1996).
31. G. G. Amatucci, J-M. Tarascon, D. Larcher, and L. C. Klein, *Solid State Ionics* **84,** 169 (1996).
32. G. Ceder, M. K. Aydinaol, and A. F. Kohan, *Comput. Mater. Sci.* **8,** 161 (1996).
33. G. Ceder, Y. M. Chiang, D. R. Sadoway, M. K. Aydinol, Y. I. Jang, and B. Huuny, *Nature* **392,** 695 (1998).
34. C. Delmas and I. Saadoune, *Solid State Ionics* **53–56,** 370 (1992).
35. T. Ohzuku, A. Ueda, M. Y. Nagayama, and H. Komori, *Electrochim. Acta* **38,** 1159 (1993).
36. T. Ohzuku, A. Ueda, and M. Kouguchi, *J. Electrochem. Soc.* **142,** 4033 (1995).
37. J. R. Dahn, E. W. Fuller, M. Obrovac, and U. Von Sacken, *in* "Recent Advances in Rechargeable Lithium Batteries," (J-M. Tarascon, Ed.), *Solid State Ionidcs* **69,** 265 (1994).
38. Yuan Gao, M. V. Yakovleva, and W. B. Ebner, *Electrochem. Solid State Lett.* **1,** 117 (1998).